Limitations and Potential of Satellite Imagery to Monitor Environmental Response to Coastal Flooding

Elijah Ramsey III[†], **Dirk Werle**[‡], **Yukihiro Suzuoki**[§*], **Amina Rangoonwala**[††**], and **Zhong Lu**[‡‡]

www.cerf-jcr.org

[†]U.S. Geological Survey
National Wetlands Research Center
700 Cajundome Boulevard
Lafayette, LA 70506, U.S.A.
ramseye@usgs.gov

[‡]AERDE Environmental Research
Box 1002, Halifax, NS, Canada, B3J 2X1

[§]ASci Corporation, Inc.
700 Cajundome Boulevard
Lafayette, LA 70506, U.S.A.

[††]IAP World Services, Inc.
700 Cajundome Boulevard
Lafayette, LA 70506, U.S.A.

[‡‡]U.S. Geological Survey
Earth Resources Observation and Science
  Center & Cascades Volcano Observatory
1300 SE Cardinal Court
Vancouver, WA 98683, U.S.A.

ABSTRACT

RAMSEY, E. III; WERLE, D.; SUZUOKI, Y.; RANGOONWALA, A., and LU, Z., 2012. Limitations and potential of satellite imagery to monitor environmental response to coastal flooding. *Journal of Coastal Research,* 28(2), 457–476. West Palm Beach (Florida), ISSN 0749-0208.

Storm-surge flooding and marsh response throughout the coastal wetlands of Louisiana were mapped using several types of remote sensing data collected before and after Hurricanes Gustav and Ike in 2008. These included synthetic aperture radar (SAR) data obtained from the (1) C-band advance SAR (ASAR) aboard the Environmental Satellite, (2) phased-array type L-band SAR (PALSAR) aboard the Advanced Land Observing Satellite, and (3) optical data obtained from Thematic Mapper (TM) sensor aboard the Land Satellite (Landsat). In estuarine marshes, L-band SAR and C-band ASAR provided accurate flood extent information when depths averaged at least 80 cm, but only L-band SAR provided consistent subcanopy detection when depths averaged 50 cm or less. Low performance of inundation mapping based on C-band ASAR was attributed to an apparent inundation detection limit (>30 cm deep) in tall *Spartina alterniflora* marshes, a possible canopy collapse of shoreline fresh marsh exposed to repeated storm-surge inundations, wind-roughened water surfaces where water levels reached marsh canopy heights, and relatively high backscatter in the near-range portion of the SAR imagery. A TM-based vegetation index of live biomass indicated that the severity of marsh dieback was linked to differences in dominant species. The severest impacts were not necessarily caused by longer inundation but rather could be caused by repeated exposure of the palustrine marsh to elevated salinity floodwaters. Differential impacts occurred in estuarine marshes. The more brackish marshes on average suffered higher impacts than the more saline marshes, particularly the nearshore coastal marshes occupied by *S. alterniflora.*

ADDITIONAL INDEX WORDS: *Environmental Satellite (Envisat) advanced synthetic aperture radar (ASAR), Advanced Land Observing Satellite (ALOS) phased array–type L-band synthetic aperture radar (PALSAR), Land Satellite (Landsat) Thematic Mapper (TM), inundation mapping, coastal marsh dieback.*

www.JCRonline.org

INTRODUCTION

Emergency response agencies and environmental resource managers require similar geospatial products. Emergency responders need to monitor coastal flooding of communities, and resource managers need to monitor the status and trends of ecosystems. The former have come to rely on the all-weather mapping capabilities of satellite sensors equipped with synthetic aperture radar (SAR), among other tools, for the rapid detection and monitoring of coastal flooding to minimize loss of lives and property. The latter have used synoptic observations by optical satellite sensors, such as the Land Satellite (Landsat) Thematic Mapper (TM), to assess the status and trends of marsh and wetland forests dominantly responding to the temporal and spatial variation in flood extent, duration, and depth. While the requirements for timely and expedient acquisition of remote sensing data and delivery may differ for emergency response and resource management situations, there is a common need for reliable and consistent access to all types of remote sensing data.

Flood extent mapping has become a routine and even operational activity in coastal marsh and forested wetland landscapes (Lu and Kwoun, 2008; Ramsey, 1998, 2005), especially during and after extreme storm events.

Satellite-based observations of long-term effects of flooding on natural vegetations are less common, however, and the usefulness of such observations requires further study. As reported in Ramsey *et al.* (2009b), the combined use of the Environmental Satellite (Envisat) advanced synthetic aperture radar (ASAR) imagery and Landsat TM optical imagery provided synergistic observations to document the extent of the coastal surge accompanying Hurricane Ike (2008) and a resultant marsh dieback event. The dieback was directly attributed to prolonged water logging and elevated salinity levels. This connection illustrated how inundation monitoring with frequent satellite radar observations, combined with the first available cloud-free optical data (*e.g.,* from Landsat TM), can provide direct links between the vegetation condition and the primary physical forces controlling it.

The Hurricane Ike example (Ramsey *et al.,* 2009b) also illustrated the reliance of emergency and environmental responses on frequent data collection. In environmental response, the necessary collection frequency is determined by the nature of the causal forces of change and the sensitivity of the environment. The frequency of the data collection determines whether the dynamics of the feature of interest are either captured or missed (Klemas, 2005). Detecting change brought on by sudden events such as severe storms, floods, and fire requires timely data collection before and after the events. Not knowing the timing of severe events requires collection to be consistent enough to provide relevant baseline data to enhance change detection. Similarly, detecting and quantifying long-term environmental trends for coastal resource monitoring requires strategic collection that is consistent and often enough to capture important changes in the coastal resource. For example, by the time a marsh dieback event was identified along the central Gulf of Mexico (GOM) coast, the affected area was extensive, in effect threatening the viability of the coastal resources (Ramsey and Rangoonwala, 2006). The marsh dieback did not happen suddenly, but the lack of a strategic data collection and mapping program, combined with the subtle and progressive change, delayed dieback detection until it became acute and highly visible. Short-term and long-term environmental responses, both of which can be dramatic, require ecosystem status indicators, measurable from coupled SAR and optical satellite data, collected strategically to promote rapid change detection and early detection of adverse regional coastal resource impacts.

Our research goal is to improve the strategic observation of the central GOM coastal regions of Louisiana through the use of combined satellite-based optical and SAR imagery and products. The objective of this study is to document the ability of L-band and C-band satellite SAR data to capture the causal agent of coastal marsh dieback and the ability of multispectral optical data to detail the near-immediate impact on palustrine and estuarine marshes in the central GOM coastal region. A previous study provided clear evidence that linked marsh dieback to the flood extent of storm surge from Hurricane Ike in the SW coastal region of Louisiana (Ramsey *et al.,* 2009b). In the current study, we apply those techniques over the entire Louisiana coast. Although both studies are limited to storm-surge flood events and opportune image collection, we extended previous results to increase quantification of (1) marsh impact

severity and (2) storm-surge mapping success with respect to SAR collection timing and wavelength. We attempt to directly relate the dieback to storm-surge inundation extent and to link inundation extents and dieback to marsh type.

STUDY AREA

The study area for Hurricanes Gustav and Ike impacts included coastal wetlands stretching from the western Chenier to the eastern Deltaic plains of coastal Louisiana, located in the north-central Gulf of Mexico (GOM; Figure 1). The Deltaic Plain was formed and is primarily sustained by direct deposition of Mississippi River sediments, while the Chenier Plain primarily depends on current-related reworking of sediments from the Atchafalaya River (USACE, 2006). Relationships between water and sediment give rise to highly permeable sand and shell (Chenier) barriers in the west and barrier islands in the east that protect extensive backbarrier marshes extending inland 6 to 24 km, commonly at less than 1.5 m above mean sea level, with slopes of less than 0.2 m per km (Chabreck, 1970).

The Louisiana coastal marsh zone is predominantly underlain by frequently saturated soils. In this zone, subsurface faulting can produce surface subsidence that results in marsh submergence and fragmentation and ultimately the formation of permanent water bodies (Kiage *et al.,* 2005; Morton *et al.,* 2005). In addition, hurricanes scour the marsh, creating small water bodies (Neyland, 2007) and pushing water with elevated salinity into fresh marshes, which causes salt burn in those areas (Neyland, 2007; Ramsey *et al.,* 2009b). Aggravating these detrimental impacts are channels and levies constructed to provide transport conduits and impoundments constructed as waterfowl sanctuaries that impede overland flow. These structural impediments can lengthen exposure of marsh to water with elevated salinity and, in the case of intense rainfall accompanying storm events, prolong inundation and promote water logging that can advance marsh alteration and deterioration. The combination of low topographic relief, poorly drained soils, tectonic activity, and flow impedance creates a spatially complex hydrologic landscape.

METHODS

Image Data Collection, Calibration, and Registration

We used SAR and TM scenes collected before and after the landfalls of Hurricane Gustav on 1 September 2008 at 1500 Coordinated Universal Time (UTC; Beven and Kimberlain, 2009) and Hurricane Ike on 13 September 2008 at 0700 UTC (Berg, 2009; Figure 1). Prehurricane SAR scenes were selected from the summer months to minimize differences connected to marsh seasonality and to best represent periods of normal sea levels and tidal flushing. Two adjacent SAR scenes (Figure 2a) and five adjacent TM scenes (Figure 2c) were required to cover the entire Louisiana coast (Tables 1 and 2).

SAR coverage was obtained by the phased array–type L-band SAR (PALSAR) sensor aboard the Japanese Advanced Land Observing Satellite (ALOS) and the C-band advanced SAR (ASAR sensor onboard the European Space Agency's Agency Environmental Satellite (Envisat. PALSAR scenes were
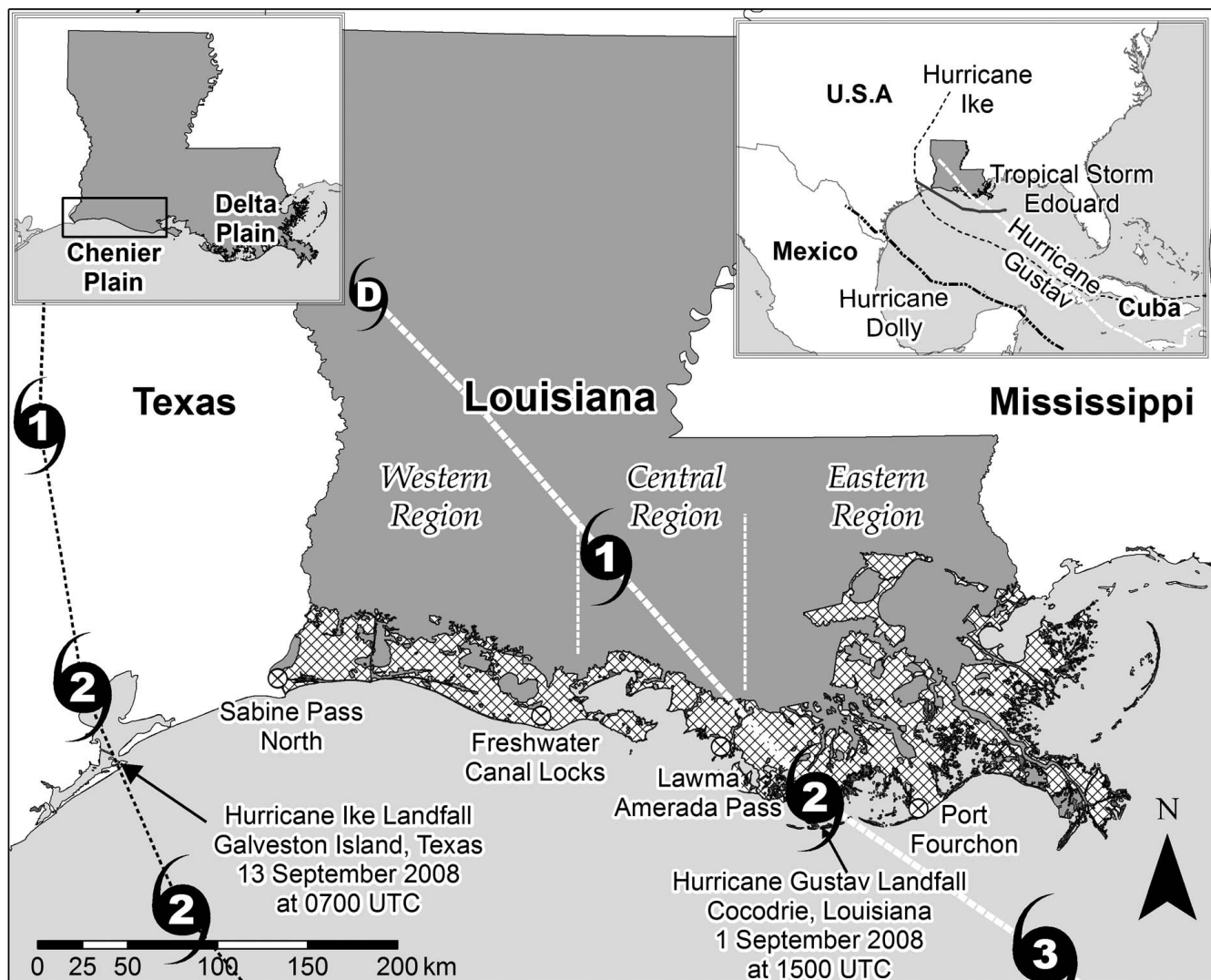
Figure 1. Study area covering the eastern, central, and western coastal regions of Louisiana. Also illustrated are the paths and Saffir-Simpson Hurricane Wind Scale categories (numbers inside hurricane symbols) assigned along the paths of Hurricanes Gustav and Ike (D refers to tropical depression). The inset shows the paths of Hurricanes Dolly, Gustav, and Ike and Tropical Storm Edouard in the Gulf of Mexico. The hatched pattern signifies the coastal zone extent.

collected over eastern Louisiana in wide area observation mode (burst mode 1) at a nominal spatial resolution of 100 m and incidence angles of 18° in the near range to 43° in the far range of the imaged swath (Figure 2 and Table 1). Two PALSAR scenes with horizontal transmit and receive (HH) polarization were radiometrically calibrated to the sigma naught backscatter coefficient (σ_0) with MapReady Remote Sensing Software available at the Alaska Satellite Facility website (2011). The ASAR scenes were collected over eastern and western Louisiana in wide swath mode at a nominal spatial resolution of 150 m and incidence angles of 17° in the near range to 42° in far range of the imaged swath (Figure 2 and Table 1). Five ASAR scenes with vertical transmit and receive (VV) polarization were transformed to σ_0 estimates (Lu and Kwoun, 2008). The σ_0 calibrations allowed scene-to-scene comparability. The 2007 and 2008 TM images collected during cloud-free

conditions were obtained from the U.S. Geological Survey (USGS) Earth Resources Observation and Science Center (Table 2). TM data acquisitions were restricted to the Landsat 5 because of problems with the scan line corrector in the enhanced TM sensor onboard the Landsat 7.

All satellite data were registered to a Landsat TM Lambert conformal conic (LCC) 25-m spatial resolution base image. The LCC projection eliminated problems of multiple Universal Transverse Mercator zones and matched the Louisiana State Plane Coordinate System defined by two standard parallels separated by 1.5° latitude, a central meridian, and a false northing and easting (WGA84 geoid). Applying State Plane parameters, we found that areas projected in the LCC and the Albers equal-area conic differed by less than 0.01%. In addition, the base TM projection was assessed by comparison to direct USGS digital orthophoto quarter quadrangles (DOQQs).
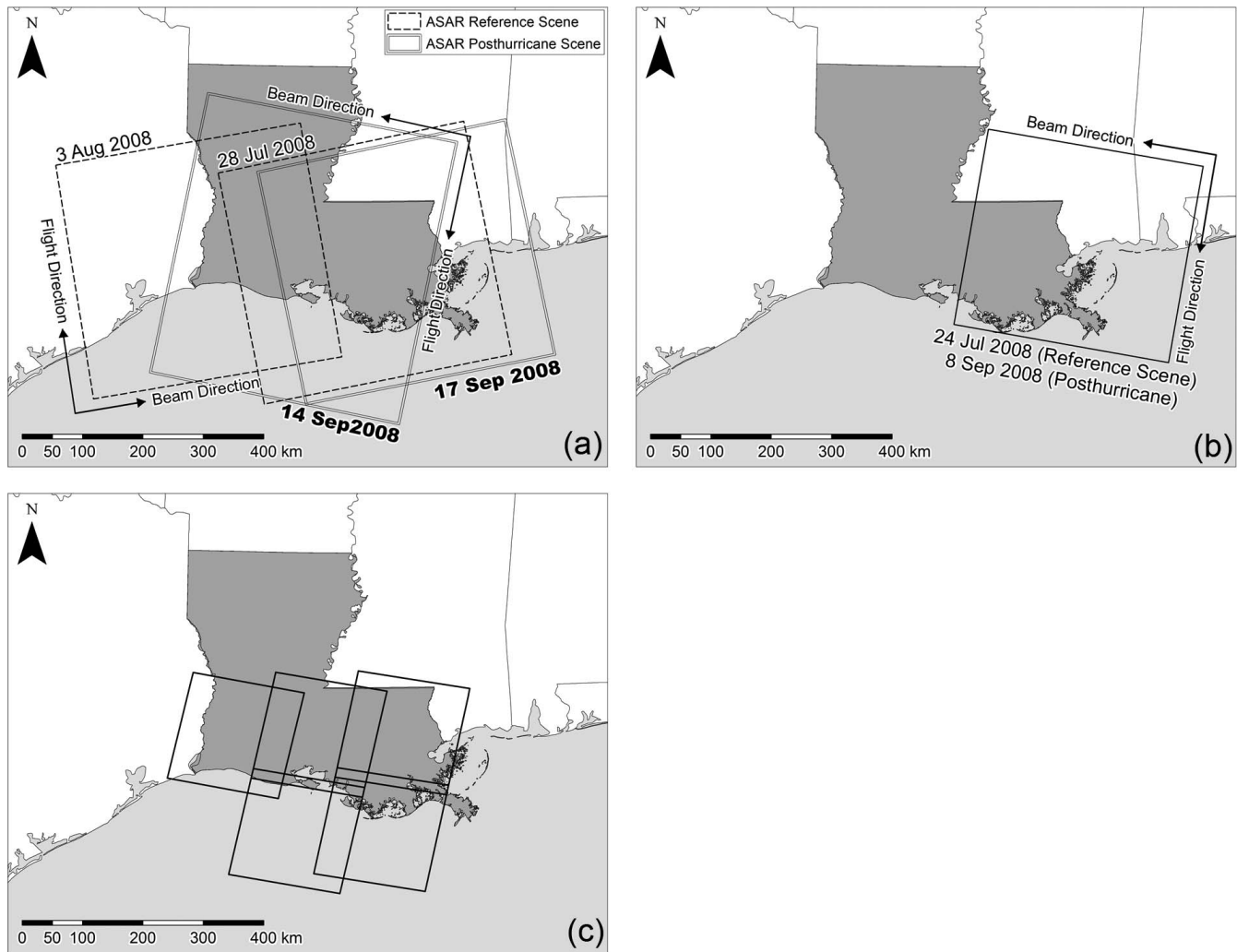
Figure 2.   Coverage locations and extents of satellite-based radar scenes and optical images used in this study. Data include (a) advanced synthetic aperture radar (ASAR) data acquired by the Environmental Satellite spacecraft, (b) phased array–type L-band SAR data acquired by the Advanced Land Observing Satellite, and (c) Land Satellite Thematic Mapper 5 images. Scenes skewed left were acquired during ascending orbital passes, and scenes skewed right were acquired during descending orbital passes of the satellite.

Table 1.   *Specifications of satellite radar scenes acquired before and after Hurricanes Gustav and Ike.*

Sensor	Polarization	Date	Time (UTC)	Orbit	LA Coastal Zone
Before					
ASAR/WS	VV	4 September 2007	0409	Ascending	Western
PALSAR/WB1	HH	24 July 2008	1627	Descending	Eastern
ASAR/WS	VV	28 July 2008	0401	Ascending	Eastern
ASAR/WS	VV	3 August 2008	0413	Ascending	Western
After					
PALSAR/WB1	HH	8 September 2008	1628	Descending	Eastern
ASAR/WS	VV	14 September 2008	1611	Descending	Western
ASAR/WS	VV	17 September 2008	0358	Ascending	Eastern

ASAR = advanced synthetic aperture radar, PALSAR = phased array–type L-band synthetic aperture radar, WS = wide swath mode, WB1 = wide beam burst mode 1, VV = vertical transmit–vertical receive, HH = horizontal transmit–horizontal receive, LA = Louisiana.

Table 2. *Specifications of Landsat Thematic Mapper scenes acquired before and after Hurricanes Gustav and Ike.*

| | Maximum Cloud Cover | |
Location	(%)	Data Acquisition Date
Prehurricane images		
Eastern	0	6 April 2007
Central	0	29 April 2007
Western	10	20 April 2007
Posthurricane images		
Eastern	1	1 October 2008
Central	4	22 September 2008
Western	1	29 September 2008

Rectification errors of the base TM (projected in LCC) to the DOQQs were most often less than 0.5 pixels. Registration errors of the base TM image to all satellite scenes ranged between 0.2 and 0.5 pixels.

Analysis of Storm-Surge Hydrographs

Coastal surge timing and height records were obtained from operational data interactive navigation of the National Oceanic and Atmospheric Administration's Center for Operational Oceanographic Products & Services (NOAA CO-OPS, 2009) for four hydrologic stations. These are located along the eastern (Port Fourchon and Lawma Amerada Pass), central (Freshwater Canal Locks), and western (Sabine Pass North) Louisiana coast (Figures 1 and 3).

Inland water-level data for calibrating and validating the inundation maps were obtained from the Strategic Online Natural Resources Information System (SONRIS, 2010) of the Louisiana Department of Natural Resources. Most inland hydrologic sites are part of the Coastwide Reference Monitoring System (CRMS). Many of these hydrologic records were incomplete for the period before, during, and after the passage of Hurricanes Gustav and Ike. Avoiding incomplete hydrologic records, we gathered data from stations in the western, central, and eastern coastal regions (NOAA CO-OPS, 2009; Figure 4). Water levels above the ground surface of marsh (at 0 m) were compared to change-detected presence or absence of persistent surge waters when SAR data collections were acquired.

With respect to the inundation analyses, the comparability of image products that are composites of spatially integrated ground elements (pixels; 150-m spatial resolution, in this case) with point measurements (water-level recorder locations) can be an issue (*e.g.,* see Fisher and Mustard, 2007). This spatial incompatibility—particularly in highly dynamic situations occurring in heterogeneous environments, such as surge flooding and recession in complex marsh systems—may diminish the reliability of the assessment method. Alternatively, water-level recordings can be a source of inundation validation error. Accurate determination of surface flooding, particularly when surface water levels are low (*i.e.,* <10 cm), requires highly accurate ground-surface and water-level elevations and reliable functioning of the water-level recorders. Inconsistencies in any factors related to the water-level recordings and scale incompatibilities may also limit the validity of the SAR-based inundation assessments. To improve the calibration and validity of the SAR inundation results, the assessments incorporated suitable adjacent marsh within a 150-m radius (nominal ASAR ground resolution) surrounding the hydrologic sites. If there was a high density of flood occurrences within the 150-m radius, we concluded that the site was flooded.

Permanent Water Body Delineation

In order to minimize confusion among wind-roughened water surfaces, flooded marsh, and nonflooded marsh, permanent water bodies were defined within the study area. Location and extent of permanent inland coastal waters obtained from the Louisiana Oil Spill Coordinator's Office (LOSCO, 2007) were updated with 13 TM images collected from 2006 to 2008 before Hurricane Gustav (western region: 4 June 2006; 20 April and 10 and 26 August 2007; and 18 February, 15 March, and 27 July 2008; central region: 13 June 2006; 29 April 2007; and 18 June 2008; and eastern region: 6 June 2006; 6 April 2007; and 13 July 2008). These TM images were registered to the same LCC-projected TM base image used for the SAR scene registration. LOSCO open-water polygon coverage was superimposed on the suite of TM images, and areas of omission between the vector coverage and the water bodies on the TM images were determined. Water bodies omitted on the LOSCO coverage that were at least 40 km^2 and exhibited spatial and temporal consistency on the TM images from 2006 up to the hurricanes of 2008 were added to the LOSCO permanent water bodies mask. Permanent water bodies were excluded from the SAR change-detection products. In addition, a coastal extent vector was used to exclude offshore waters (LOSCO, 2007). Location errors in the coastal vector were found in rapidly changing and spatially complex deltaic marshes, such as the Mississippi River, Atchafalaya, and Wax Lake deltas (Figure 4).

Mapping Inundation

In order to detect changes related to the passage of Hurricanes Gustav and Ike, calibrated reference (normally prehurricane) and posthurricane SAR scenes were required. The reference SAR scenes were chosen from within the same season to minimize change-detection differences caused by vegetation phenology and at times that avoided atypically elevated sea levels and coastal flooding (*e.g.,* Hurricane Dolly and Tropical Storm Edouard; Figure 5). These criteria helped ensure the change-detection algorithm could capture subcanopy flooding specifically associated with Hurricanes Gustav and Ike.

Each posthurricane scene was paired with an appropriate L-band or C-band reference scene based on common HH or VV polarization to eliminate change artifacts associated with polarization differences across the SAR imagery. A logarithmic ratio of the reference and posthurricane scenes resulting in a positive decibel difference, indicating lower intensities after the hurricanes than before. In these marshes, it (dB differences) also indicated possible inundation. To help limit noise and better discriminate flooded from nonflooded marsh, the SAR-based change-detection algorithm incorporated a 5 × 5 pixel internal Kuan speckle filter to dampen noise while preserving edges and shape. In addition, minimum change-detection thresholds were applied that relied on identifying
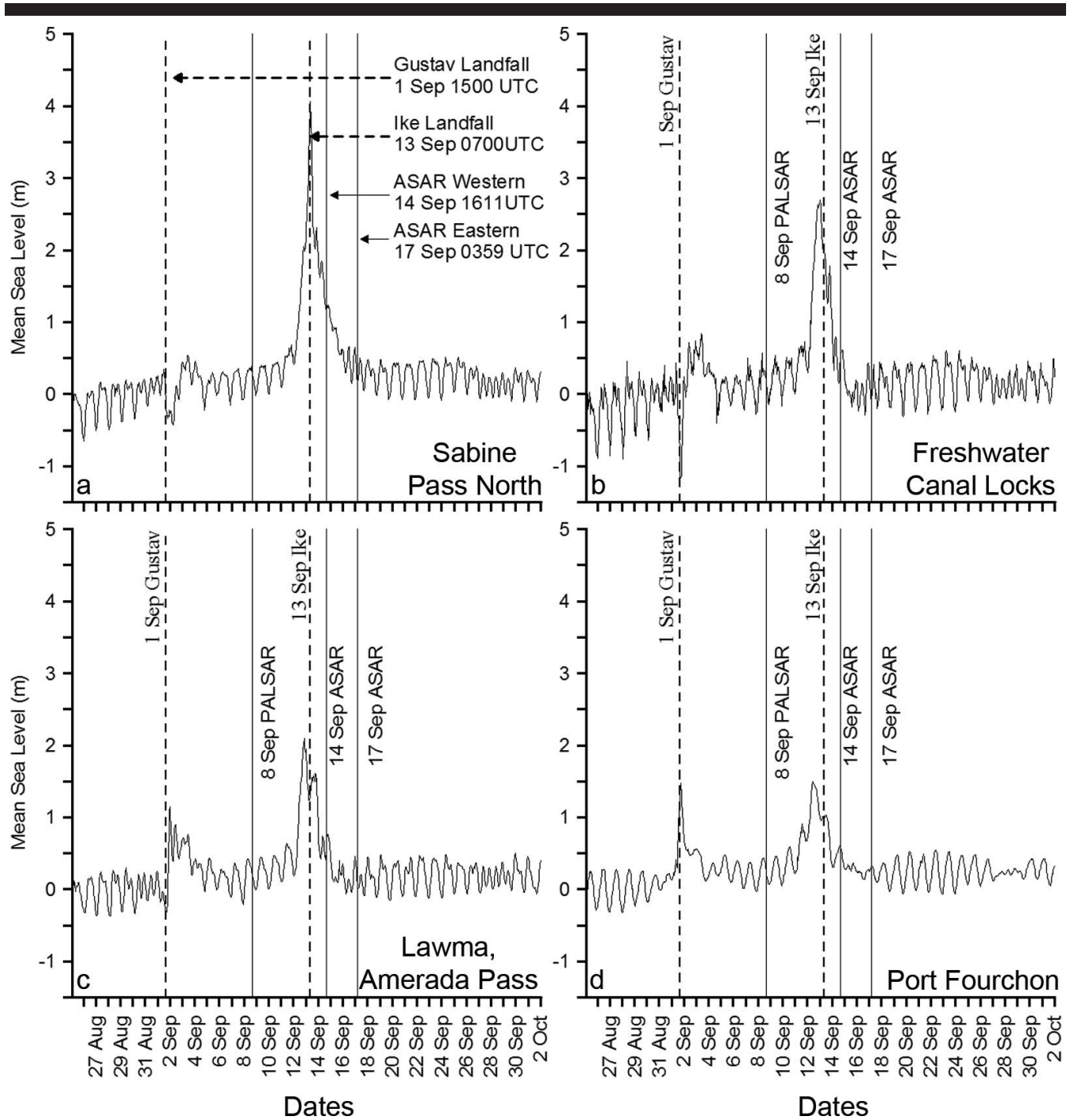
Figure 3. Hydrographs showing water levels (NOAA CO-OPS, 2009) along the Louisiana coast (see Figure 1): (a) western station, Sabine Pass North; (b) central station, Freshwater Canal Locks; and eastern stations, (c) Lawma Amerada Pass and (d) Port Fourchon.

inflections on plots of SAR backscatter versus threshold value and visual interpretation, guided by inland water-level fluctuations, to discriminate flooded from nonflooded marsh (Ramsey *et al.*, 2011). Once appropriate threshold values were obtained, we mapped the surge extent occurring at the time of posthurricane SAR collection along the entire Louisiana coast.

Reference Scene Comparison

The dependency of the SAR inundation mapping performance on the reference scene selection was evaluated at one posthurricane SAR scene date point. In the western region, we replaced the reference SAR scene—from 3 August 2008—with
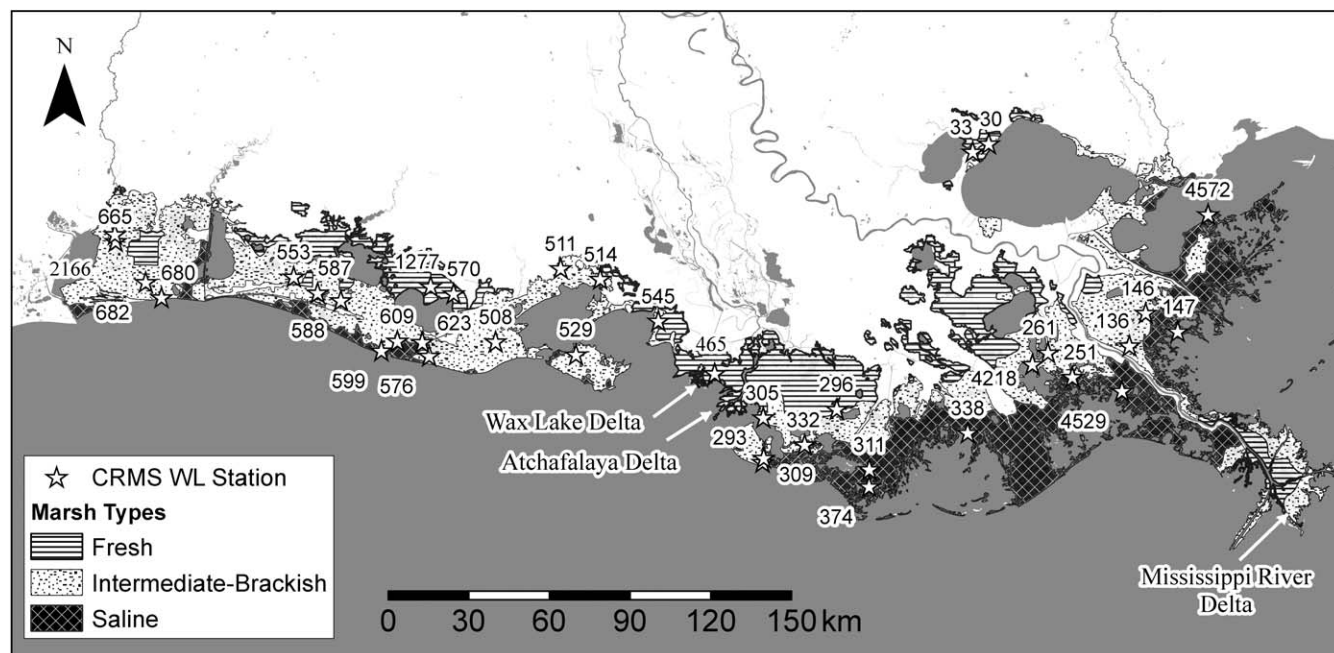
Figure 4. Stations within the Coastwide Reference Monitoring System, where inland water-level data were acquired (made available through SONRIS, 2010). Four patterns show fresh, intermediate, brackish, and saline marsh zones.

a scene acquired on 4 September 2007. We then compared the results of these two separate inundation–detection analyses.

Dieback Extent and Marsh Type

Using the 2007 Louisiana Coastal Marsh–Vegetative Type Map (Sasser *et al.,* 2008) as a guide, we included fresh marsh in the palustrine wetland class and combined intermediate, brackish, and saline marshes into the estuarine marsh class to generalize the comparisons and to better align with national wetland classification systems (Klemas *et al.,* 1993). At times, components of the estuarine marsh, including intermediate–brackish and saline marshes, were separately evaluated with respect to impact severity. Swamps and upland classes were excluded from our analysis (Figure 4). Combined, the ASAR scenes and TM images covered 8688 km² of estuarine and 3290 km² of palustrine marshes along the entire Louisiana coast, and the PALSAR scenes covered 4994 km² of estuarine and 1928 km² of palustrine marshes along the eastern region of the coast.

Although dieback was visually apparent on the posthurricane TM images, to assess its extent we needed to standardize the multispectral values of the imagery to a single green-biomass indicator. We achieved standardization by performing a simple ratio transformation (near infrared to red) of vegetation index (VI) values to derive the single green-biomass estimator. Transformation of the TM-based VI values helped minimize atmospheric and illumination differences between prehurricane and posthurricane images and provided a single index more conducive to analyzing change (Ramsey *et al.,* 2009a). Once we transformed to VI values, we produced a single image to capture green-biomass differences between prehurricane and posthurricane images. Only positive differences, indicated by green-biomass content that was higher before than after the storm-surge event, were considered in the dieback assessment.

We wanted not only to assess the extent of the dieback but also to estimate its severity across the landscape. In order to provide an impact severity estimate, we needed to account for natural variability in green-biomass content outside the context of hurricane impacts. In order to relate the change magnitude to the local prehurricane green-biomass levels, we combined prehurricane–posthurricane change VI values with prehurricane absolute VI values and then performed an unsupervised Iterative Self-Organizing Data Analysis Technique (ISODATA) classification (PCI Geomatics, 1998; Tou and Gonzalez, 1974) on the entire dataset. Resultant data clusters were grouped into impact classes based on modal features in the difference frequency histogram. The prehurricane and change VI means and standard deviations (SDs) were calculated for each impact class. The class mean was calculated as the sum of cluster means divided by the number of clusters comprising the impact class. The variance per impact class was calculated by multiplying the sum of the squared SD per classification cluster (comprising each class) by the reciprocal number of clusters squared (Bevington, 1969). The SD per class was calculated as the square root of the variance estimate.

Another aim of our study was to obtain a measure of severity of the surge impact specific to palustrine and estuarine marshes. Our classification of change magnitudes (*via* ISODATA) did not include marsh type; therefore, we overlaid the 2007 Louisiana Coastal Marsh–Vegetative Type Map (Sasser *et al.,* 2008) onto our initial image indicating green-biomass
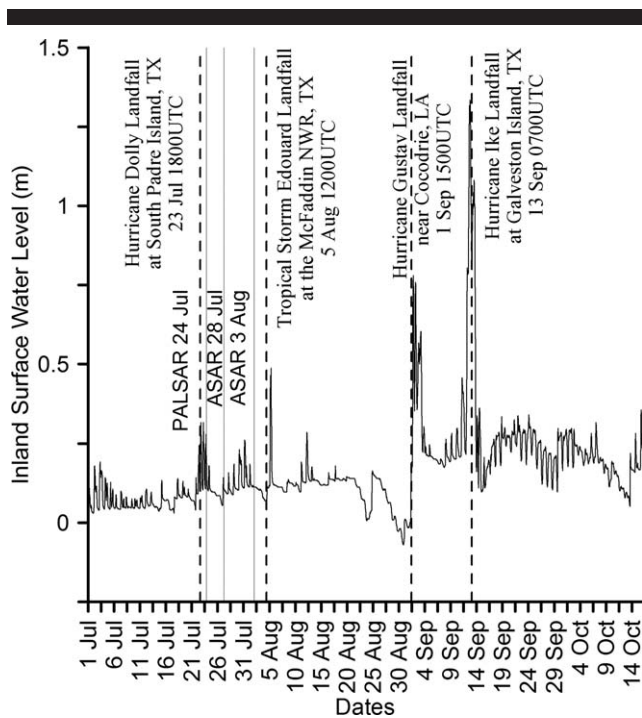
Figure 5. Hydrologic data from 1 July to 20 October 2008 at station CRMS0465 in the Coastwide Reference Monitoring System (CRMS; SONRIS, 2010). The hydrograph shows water-level peaks associated with Hurricane Dolly (23 July), Tropical Storm Edouard (5 August), Hurricane Gustav (1 September), and Hurricane Ike (13 September). (See Figure 1 for storm paths and Figure 4 for the CRMS station location.) Reference scene collection dates are shown as solid lines.

changes. We then introduced our change-magnitude classification to map the severity and extent of dieback specific to each marsh type.

RESULTS

Coastal Surge Data

Analysis of the hydrograph data show that the direct impacts of elevated salinity related to storm surge from Hurricane Gustav were limited to the east-central and eastern regions of coastal Louisiana (Figure 3). Storm surge associated with the landfall of Hurricane Gustav was clearly indicated only on the hydrographs for the eastern region (Figures 3c and d). A hydrograph for Amerada Pass (Figure 3c), at the borderline of the central and eastern regions, showed a storm-surge peak at landfall of Hurricane Gustav, but the surge was not recorded 75 km to the west at Freshwater Canal Locks (Figure 3b). In the central and western regions, offshore flow of coastal water occurring upon landfall Hurricane Gustav was reported as a drawdown on the hydrographs (Figures 3a and b). In contrast, storm surge associated with the passage of Hurricane Ike impacted the entire Louisiana coast (Figure 3). Storm-surge peak heights increased from east to west, while time delays between the storm-surge peak and the SAR scene collection decreased. The time delay was particularly pronounced in the

eastern coastal region covered by the 17 September 2008 eastern ASAR scene, which was acquired 16 days after Hurricane Gustav and 4 days after Hurricane Ike (Figures 2, 3c, and 3d).

Reference Scenes and Thresholds for Detecting Changes in Inundation

SAR collection times during the summer season ahead of Hurricanes Gustav and Ike overlain onto a coastal hydrograph obtained from NOAA CO-OPS (2009) yielded the following insights. The presence of Hurricane Dolly and Tropical Storm Edouard in the Gulf of Mexico from mid-July to early August 2008 abnormally elevated coastal sea levels (Figures 1 and 5). Hydrographs depicting inland conditions from 15 July to 13 October indicated that elevated water levels above the surrounding marsh surface (denoting the ground surface of marsh subcanopy or 0-m water level) existed at some CRMS locations near the times of Hurricane Dolly and Tropical Storm Edouard landfall (SONRIS, 2010; Figure 6). Although pre-hurricane reference scenes collected during "typical" sea levels were preferred, the approaches of Hurricane Dolly and Tropical Storm Edouard and landfalls of Hurricanes Gustav and Ike from the latter half of August to mid-September 2008 limited our choice of reference SAR scenes. Taking into account the necessity for consistency in seasonality, only two ASAR scenes and a single PALSAR scene were available as candidate reference scenes for the change-detection analyses (Figure 5). The reference SAR scenes were collected at times of higher-than-preferred water levels.

Inundation Thresholds

The total area associated with positive change-detection results above each incremental increase of threshold magnitude was calculated for each posthurricane ASAR date (Ramsey *et al.,* 2011). Inflections in the plotted trends were examined for indications of an abrupt change in the SAR backscatter that could have been related to a change from flooded to nonflooded marsh. All five curves decreased without an obvious inflection point throughout the threshold ranges we evaluated (Figure 7). Lacking an inflection point indicating an abrupt change, choice of threshold values was guided by inland water levels and visual interpretation. Threshold magnitudes of 0.1 dB (ASAR) and 1.0 dB (PALSAR) were found to retain trends in hydrologic data recorded inland at CRMS stations and in visual interpretation of inland inundation extent.

Even though limited to a single comparison, replacement of the 3 August 2008 scene (the most appropriate reference scene) with the 4 September 2007 scene as the ASAR reference scene produced results that exhibited high agreement with inundation results based on the 3 August reference and 14 September 2008 ASAR scenes (Figure 8).

Flooding-Related Changes and Inland Water Level Records

We found that the locations of many inland hydrologic stations did not allow direct comparisons between recorded water levels and measurements of surface inundation calcu-
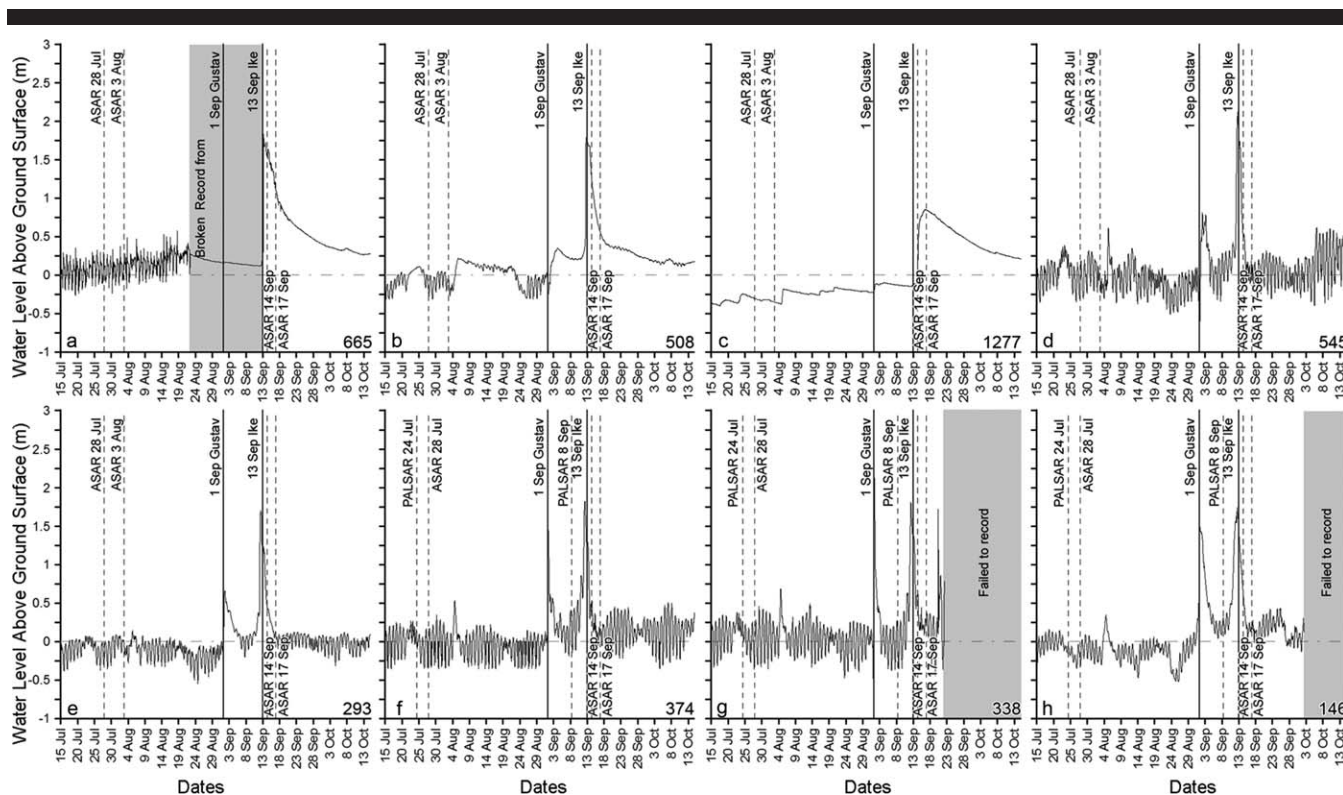
Figure 6. Hydrologic data from selected stations of the Coastwide Reference Monitoring System (CRMS; available through SONRIS, 2010) covering the eastern, central, and western coastal regions (see Figure 4 for station locations): (a) CRMS0665, (b) CRMS0508, (c) CRMS1277 (note peak delay), (d) CRMS0545, (e) CRMS0293, (f) CRMS0374, (g) CRMS0338, and (h) CRMS0146. Vertical dashed lines indicate the dates of satellite data acquisition (before and after Hurricanes Gustav and Ike), and solid lines indicate the dates of hurricane landfall. Water levels of 0 (m) designate the ground-surface height around a given data recorder.

lated with SAR data. Although locations on the marsh platform were preferred, most recording sites were located in water channels that exhibit flow dynamics different from those of the marsh platform and were separated from the marsh platform by varying distances and partial obstructions, such as levies. Many recording sites were located in a landscape of mixed marsh and forest stands or in degrading marsh containing a high proportion of open water. In the most egregious cases (*e.g.,* spatially extensive open water, degrading marsh, or mixed land covers), the incompatibility of the water-level data and the SAR data required us to discard data from these hydrologic sites or move assessment points to an adjacent area exhibiting the desired marsh extent and uniformity.

Even after removal of the most incompatible hydrologic sites, most sites were influenced by mixed land covers on the SAR imagery, various hydraulic impediments to flow, and as mentioned earlier, the possibility of inconsistencies in the water-level recordings. Increase of the assessment area to the spatial resolution of the sensor (100 and 150 m for PALSAR and ASAR, respectively) alleviated some spatial scale incompatibilities; however, remaining inconsistencies tempered direct validation of SAR-based marsh flooding with available hydrologic data. This was especially apparent in central and eastern coastal regions, where SAR-based flood detection produced scattered pockets of persistent flooding.

Even though most inland hydrologic sites were unsuitable for use in direct validation, the occurrence or absence of elevated water levels at the recording stations provided an indication of flooding in the surrounding marshes and, thus, an overall measure of the performance of SAR-based flood detection. Site-specific assessments, especially in areas of shallow water, were not as important as the assessment of trends.

Storm-Surge Extents Estimated with SAR Data

Inundation maps based on ASAR and PALSAR change-detection analyses showed prominent storm-surge flooding in the western region and isolated pockets of residual flooding in the central and eastern regions (Figure 9). Residual flood patterns differed in the eastern sector when the scene of 17 September was replaced with the scene of 14 September (both scenes acquired after Hurricanes Gustav and Ike; Figures 9c and d). There was generally low correspondence between satellite-based flood mapping using the 17 September ASAR scene and ground-based water-level measurements; however, in one area, the 17 September scene produced more reliable mapping results than those based on the 14 September scene. This area included the estuarine marsh in the eastern region, particularly in the near-shore estuarine marsh and the upper estuarine marsh located at the eastern edge of the overlap zone
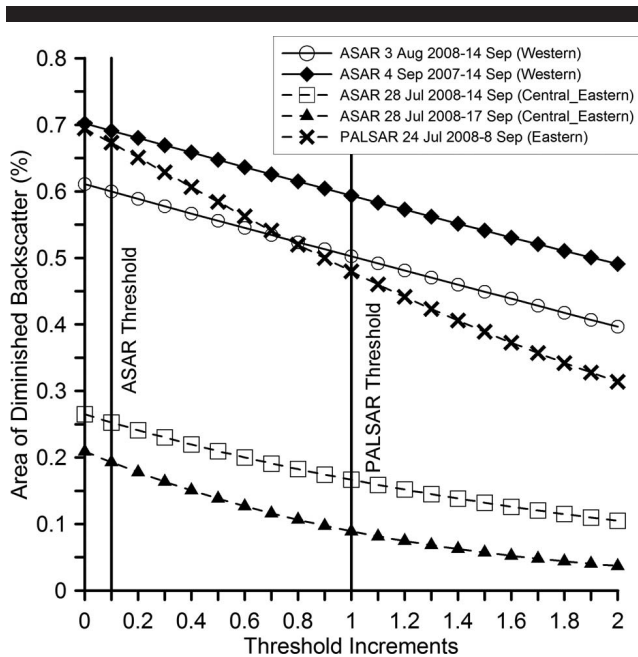
Figure 7. Positive threshold trends for detecting inundation (see Ramsey *et al.,* 2011). The area of diminished backscatter percentage refers to those marshes where the reference scene backscatter was higher than the posthurricane backscatter, indicating flooding (the reference and post-hurricane scene dates are shown in the legend). The percentage is used because each trend line is normalized by the pertinent coastal region area depicted in Figure 1. As described in the text, not all decreased backscatter indicates the occurrence of flooding; the thresholds are used to help remove those non–flood-related decreases. Trends were derived to examine whether an inflection in the trend could be used to establish the threshold. No inflections were visually apparent; however, the trends describe the relative differences in extent (intercept) and the form of the threshold increase with extent.

between the 14 September and the 17 September scenes (Figures 9c and d). Extensive flooding detected in the upper estuarine marsh using the 17 September scene was not detectable using the 14 September scene. Inland hydrologic data collected at CRMS stations within this area (CRMS0251, CRMS146, and CRMS3667) showed that shallow flooding present in this marsh on 17 September was deeper at the time of the 14 September ASAR collection. Although the 14 September ASAR scene did not extend far enough to the east to cover CRMS4572, CRMS146, CRMS147, CRMS136, and CRMS4529, data from these sites also indicate that water levels decreased from 14 to 17 September 2008. The unreliable results from the 14 September scene might be explained by the relatively high SAR backscatter exhibited in the near range, which could have decreased the contrast that would be expected between nonflooded marsh (prehurricane) and flooded marsh (posthurricane) in the ASAR scenes, thus lowering the performance of our change analysis (Ramsey *et al.,* 2011).

SAR-Based Storm-Surge Extent and Inland Hydrologic Data

Overall, correspondence of the spatial and temporal juxtaposition of ground-based water-level measurements with ASAR-based inundation results was 78% for the 14 September imagery and 67% for the 17 September imagery; correspondence was 91% with the PALSAR-based inundation results for the 8 September imagery (Figure 10).

Western Region

The highest regional correspondence of 92% was in the western region for the 14 September ASAR scene. This high correspondence was linked to the shortest time delay between the surge peak (of Hurricane Ike) and SAR data collection at 33 hours (on 14 September) and the highest surge-related water levels (1.21 ± 0.43 m; 13 September, 0800 UTC, 4.06 m at Sabine Pass North; NOAA CO-OPS, 2009; Figure 3a).

Central Region

The central region was imaged by ASAR on both 14 and 17 September at 40 and 100 hours, respectively, after the surge peak of Hurricane Ike on 13 September (Figure 3b). Even though inland measurements of water levels were higher on 14 September (0.59 ± 0.34 m) than on 17 September (0.13 ± 0.27 cm), we achieved better performance in inundation mapping with the 17 September imagery (88% correspondence with inland hydrologic data) than with the 14 September imagery (50% correspondence; Figures 10a and b).

Eastern Region

The eastern region was imaged by PALSAR 167 hours after the storm-surge peak of Hurricane Gustav and by ASAR on 14 and 17 September at 55 and 115 hours, respectively, after the Hurricane Ike storm-surge peak (Figure 3c). Correspondence between the PALSAR-based inundation data and the ground-based water-level measurements was 91%, with water levels averaging 0.22 ± 0.10 m (Figure 10c). Correspondence was 86% in the far range of the 14 September ASAR-based inundation image, with average water levels of 0.79 ± 0.17 m, and 50% in the near range of the 17 September ASAR scene, with average water levels of 0.27 ± 0.13 m.

C-band Versus L-band Inundation Mapping

Varying performance rates between PALSAR-based and ASAR-based inundation mapping offer an estimate of the canopy penetration limits of C-band sensors applied to denser estuarine marshes. At ground-based monitoring sites in the eastern region where flood occurrences were incorrectly mapped by the 17 September ASAR data, five of the six sites contained canopies of tall *Spartina alterniflora* marsh (CRMS374, CRMS338, CRMS4529, CRMS147, and CRMS4572). Of those five sites, CRMS374 and CRMS338 were within the coverage area of the 14 September ASAR scene. According to ground-based measurements, the average flood depths on 14 and 17 September (when ASAR scenes were collected) were 0.60 ± 0.08 and 0.20 ± 0.07 m, respectively. ASAR-based mapping of flood occurrences agreed with ground-measured flood occurrences on 14 September but not on 17
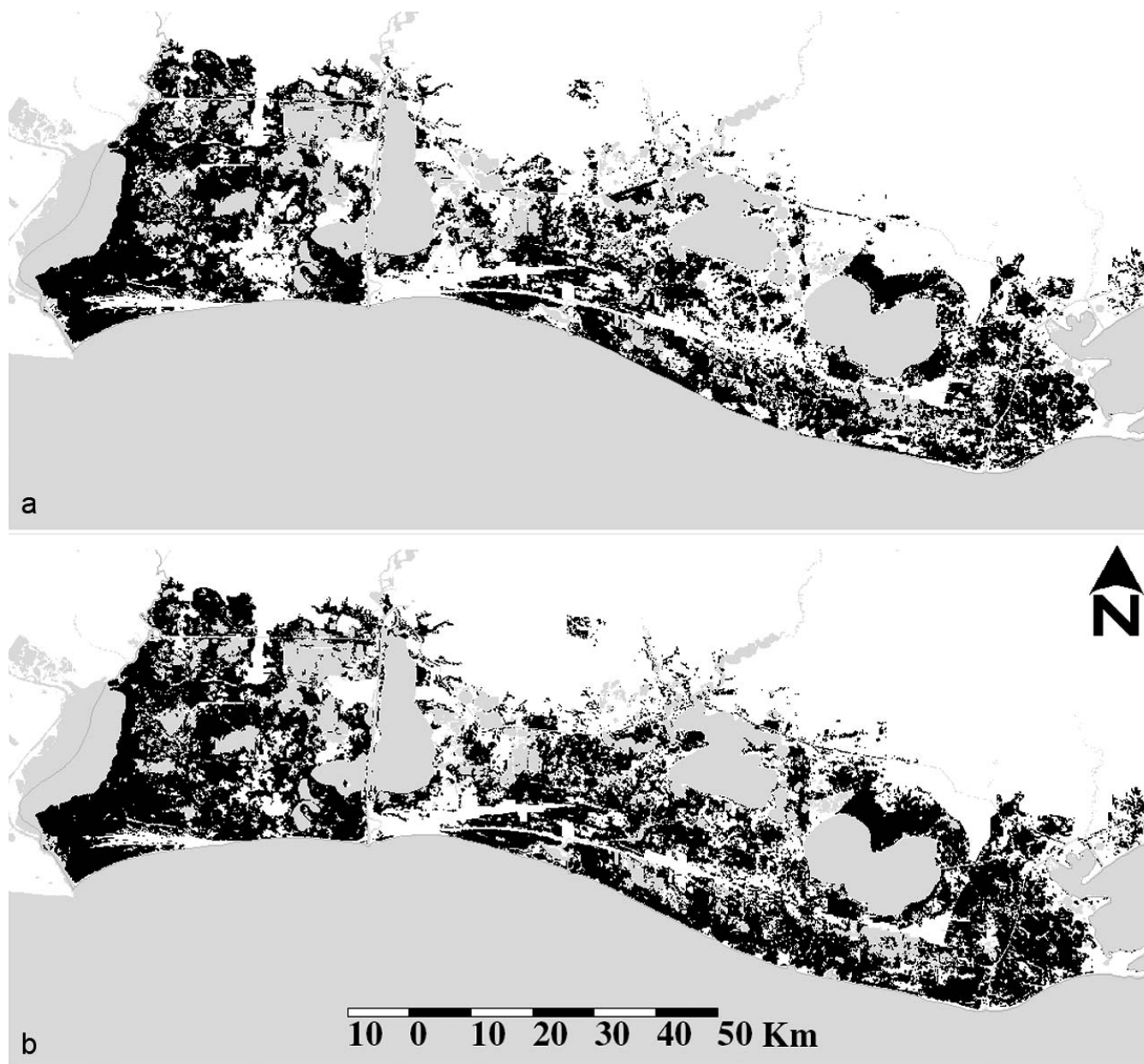
Figure 8. Comparison of inundation maps based on advanced synthetic aperture radar (ASAR) reference scenes acquired on different dates before Hurricanes Gustav and Ike. (a) Inundation based on 3 August 2008 reference and 14 September 2008 posthurricane scenes. (b) Inundation based on 4 September 2007 reference and 14 September 2008 posthurricane scenes.

September. Although evidence is not conclusive, C-band ASAR mapping of subcanopy inundation may be limited, on average, to flood depths higher than 20 to 30 cm in tall *S. alterniflora* marshes. Similarly, flood occurrences at three (CRMS374, CRMS338, and CRMS4529) of the five ground-based monitoring sites were incorrectly mapped with the 17 September ASAR scene, but occurrences were correctly mapped with the PALSAR data when depths averaged 0.10 ± 0.086 m. These results suggest increased ASAR-based mapping performance with increasing depths of subcanopy inundation (before overtopping) and the higher efficiency of L-band versus

C-band data in mapping marsh inundation, particularly in denser marshes with shallow flooding.

Dieback Extent and Marsh Type

TM images collected before and after Hurricanes Gustav and Ike transformed into VI images (Figure 11) were combined to produce four classes of VI change relative to the before VI magnitudes (Table 3). The VI classes formed spatially contiguous classes representing four classes of dieback severity within the palustrine and estuarine marshes (Figure 12 and
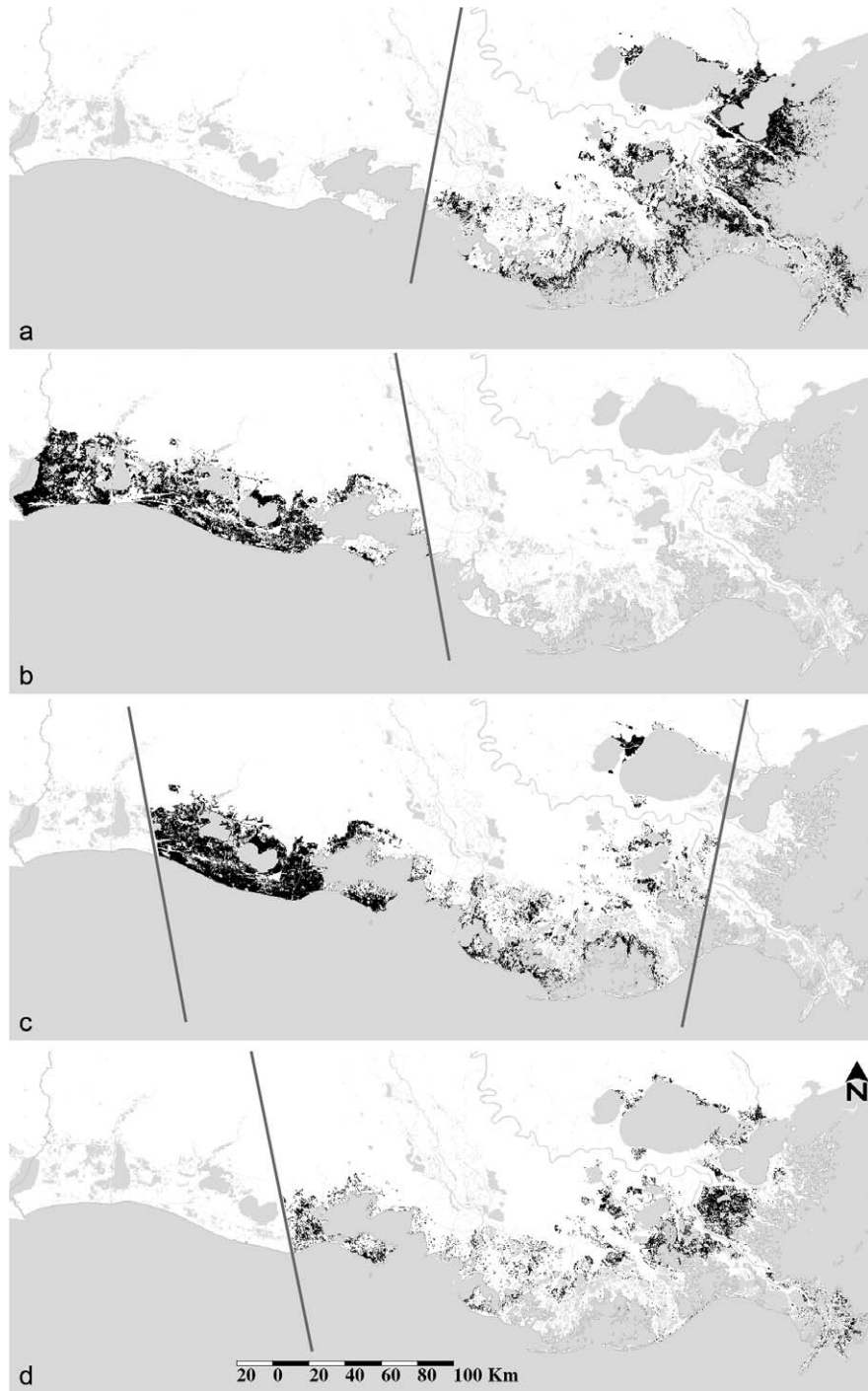
Figure 9.   Inundation maps based on advanced synthetic aperture radar (ASAR) and phased array–type L-band SAR (PALSAR) (derived from data ©2008, JAXA METI) data. Solid lines denote the limits of inundation mapping for each date. Inundation extents (shown in black) are based on (a) 24 July 2008 reference and 8 September 2008 posthurricane PALSAR scenes, (b) 3 August 2008 reference and 14 September 2008 posthurricane ASAR scenes, (c) 28 July 2008 reference and 14 September 2008 posthurricane ASAR scenes, and (d) 28 July 2008 reference and 17 September 2008 posthurricane ASAR scenes. The storm surge is prominent in the western region and is present in isolated pockets in the central and eastern regions.
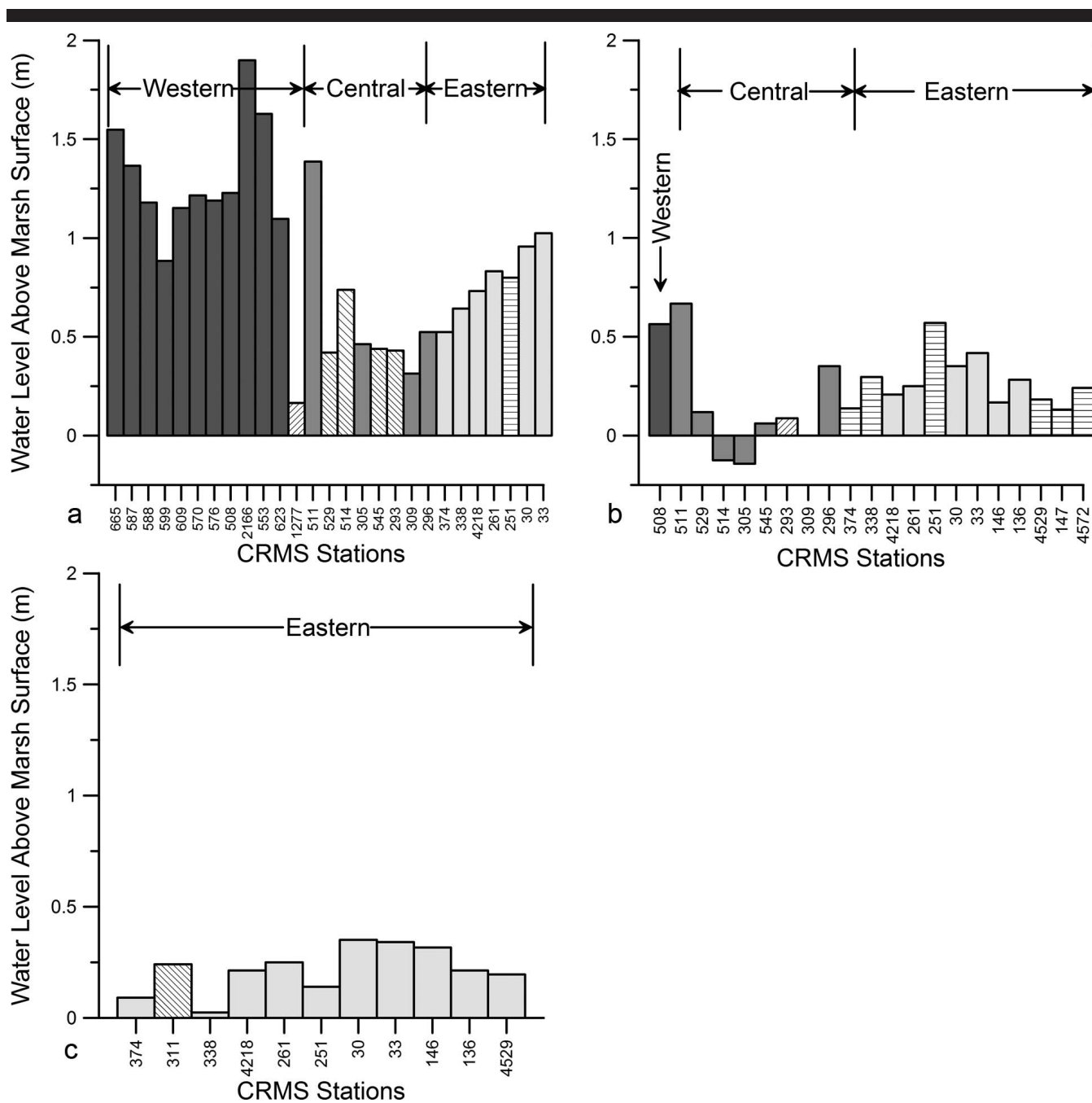
Figure 10. Water levels above the ground surface of marsh (0 m) at inland hydrologic stations (see Figure 4 for station locations) when satellite data were acquired after Hurricanes Gustav and Ike. Inundation (or its absence) was compared across the inland hydrologic data and the satellite data. The regional locations of the stations are indicated with bar shades, with dark, medium, and light gray bars indicating western, central, and eastern zones, respectively. Where inland and satellite data corresponded, solid bars are used; where they differed, lined bars are used. Water levels and correspondences based on (a) 14 September 2008 advanced synthetic aperture radar (ASAR; CRMS0146 is located just east of the scene extent), (b) 17 September 2008 ASAR, and (c) 8 September 2008 phased array–type L-band synthetic aperture radar. (See Figure 9 for inundation coverage.)

Table 4). The highest percentage of palustrine marsh dieback was associated with the low impact class, according to changes in VI values (Table 4). The low impact palustrine marshes occurred most often just inland of the estuarine marshes in the east and western regions. The second highest spatial percentage was associated primarily with an isolated inland pocket of managed palustrine marshes in the east-central coastal region. The high and severe impact marsh classes were concentrated in the central coast, where the palustrine marshes occupy the ocean-to-marsh transition.

The pattern of estuarine dieback varied in the western and eastern regions. Estuarine dieback in the eastern region was
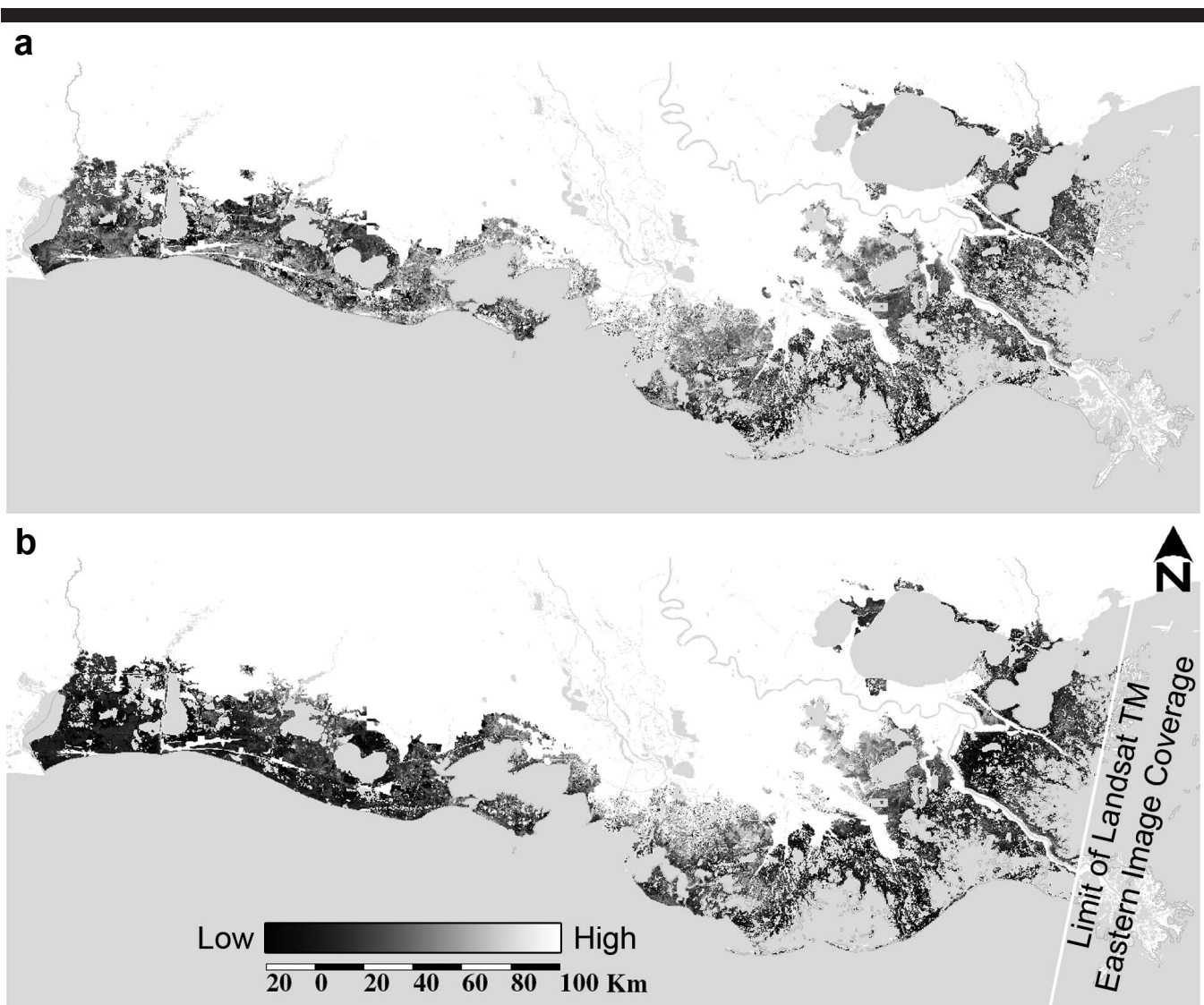
Figure 11. Maps of the vegetation indexes created from Landsat Thematic Mapper imagery acquired before and after Hurricanes Gustav and Ike, based on (a) prehurricane imagery (from April 2007) and (b) posthurricane imagery (from September and October 2008). The lighter gray colors (black progressing to white) represent increasingly higher vegetation indices.

dominantly characterized by the low impact class near shore and by moderate impact class farther inland (Table 4). In the western region, estuarine dieback was dominantly characterized by moderate impact, but some of the marshes farthest inland were characterized by low impact. The high and severe impact classes were associated with estuarine marshes found in localized pockets along the coastline in the central and western portions of the western region.

Separating the estuarine marsh into saline marsh components and intermediate–brackish components, we found that saline marshes dominated by *S. alterniflora* and occupying the nearshore in the eastern region most often displayed the low impact class of dieback (72%), followed in frequency by the moderate impact class (27%; Table 5). The remaining 1% of saline marsh was characterized by the high impact class. On

the other hand, intermediate–brackish marshes in the eastern region were equally likely (47%) to be characterized by the low and moderate impact classes, with 6% included in the high and severe impact classes.

In the marshes of the eastern region, the direct comparability of the saline and intermediate–brackish marshes was justified by their similar spatial extent. In the central and western regions, saline marshes were only 2 and 11% of the aerial extent of intermediate–brackish marshes, respectively. Even though the comparison is tenuous, saline and intermediate–brackish marshes exhibited similar patterns in the western region. About 30% of both marsh types were characterized by the low impact class, and about 60% were characterized by the moderate impact class. The saline marshes in the western region,

Table 3. *Thematic Mapper Vegetation Index (VI) Means and Standard Deviations (SDs) per Impact Class.**

Dieback Severity	Prehurricane VI Values		Pre- to Posthurricane VI Change		
	Mean	SD	Mean	SD	N
Low impact	1.90	0.05	0.30	0.06	7
Moderate impact	2.80	0.07	0.84	0.07	7
High impact	3.90	0.10	1.70	0.09	5
Severe impact	4.98	0.09	3.22	0.08	8

* The impact classes combined palustrine and estuarine marshes.

N = number of clusters aggregated *per* impact class.

however, are often dominated by *Distichlis spicata*. Although *D. spicata* is commonly called saltgrass and classified as saline, these plants are more accurately designated as brackish. Considering *D. spicata* as an intermediate–brackish marsh would result in the eastern and western dieback severities being more comparable. In

that case, it may be that marshes classified as saline are not less sensitive to elevated salinity waters but that a specific saline marsh species dominating the eastern shoreward marsh—namely *S. alterniflora*—is less sensitive to elevated salinity from storm surge than are most or all other coastal marsh species.
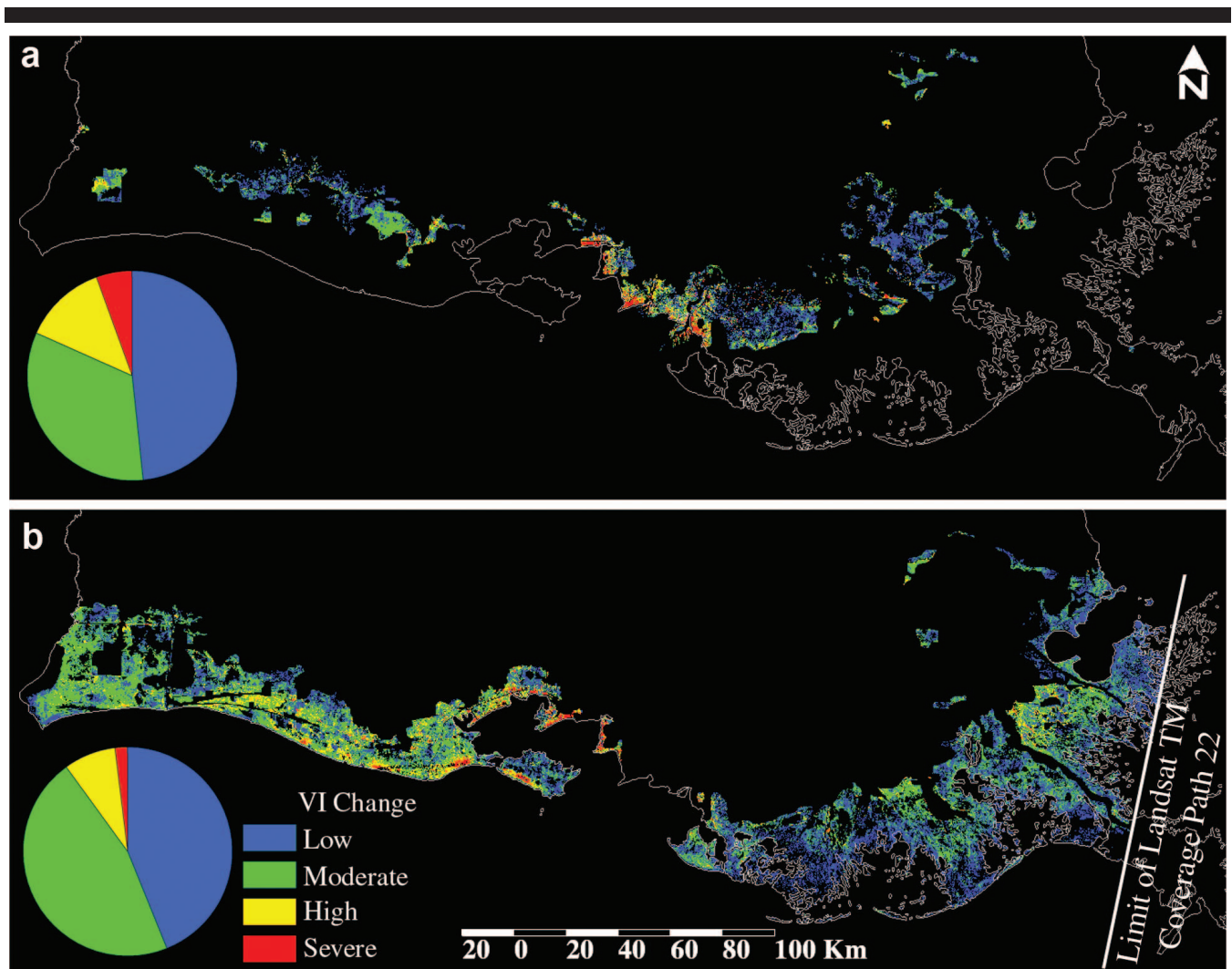
Figure 12. Magnitudes of severity in marsh dieback along the Louisiana coast indicated by prehurricane and posthurricane vegetation indexes and their differences based on Landsat Thematic Mapper imagery. (a) Spatial distribution of dieback severity in palustrine wetlands. (b) Spatial distribution of dieback severity in estuarine wetlands. (Classes of dieback severity follow those presented in Table 4.)

Table 4. *Marsh dieback severity in palustrine and estuarine wetlands of coastal Louisiana.*

Wetland Type	Dieback Severity	Area (%)	Area (km²)
Palustrine	Low impact	48	1040
	Moderate impact	33	714
	High impact	13	274
	Severe impact	6	122
	Total	100	2150
Estuarine	Low impact	44	3221
	Moderate impact	46	3378
	High impact	8	588
	Severe impact	2	145
	Total	100	7332

Storm-Surge and Dieback Relationships

The highest spatial agreement between the geographic extent of the surge-induced marsh dieback and the mapped surge flooding occurred in the western portion of the study area (Figures 9 and 12). Satellite coverage of this region was also characterized by the least lag time between storm-surge peak and data collection. By contrast, in the eastern region, timing of the SAR data collection did not align well with timing of the storm-surge peak (Figures 9 and 12). In the eastern region, the residual flooding distribution was calculated based on a PALSAR scene collected 167 hours after Hurricane Gustav and an ASAR scene collected 115 hours after the eastern storm-surge peak of Hurricane Ike.

DISCUSSION

Storm-Surge Mapping

Persistent flooding in the coastal zone brought about by storm surge from Hurricanes Gustav and Ike was mapped with reference and posthurricane Envisat ASAR and ALOS PALSAR scenes. Coastal hydrographs obtained from NOAA CO-OPS (2009) reported the storm surge from Hurricane Gustav primarily affected the eastern and more central regions and from Hurricane Ike affected the entire coast from eastern to western Louisiana. The PALSAR scene captured residual storm-surge flooding in the eastern region 167 hours after Hurricane Gustav, and ASAR scenes captured residual flooding 33, 40, and 115 hours after storm surges from Hurricane Ike in the, western, central, and eastern regions of the Louisiana coast, respectively.

In all regions, as lag time increased between storm-surge peaks and ASAR scene collection, detected inland flood extents and water levels decreased. The shortest time lags in the western region were associated with fairly spatially contiguous flooding, while increased time lapses were related to detection of highly scattered and isolated pockets of flooding in the central

and eastern regions. Although the storm surge had largely receded in the eastern and central coastal areas by the time satellite data were collected in those regions, flooding persisted in the estuarine and palustrine marshes farther inland.

Correspondence of Change-Detected Flooding and Recorded Inland Water Levels

Based on inland water levels (SONRIS, 2010) and flood extent results in the western region, ASAR-based inundation mapping performed well when average above-surface water levels were at least 79 cm. These higher correspondences may be attributed to the inverse covariance between depth increase of subcanopy inundation and decrease of SAR backscatter due to less biomass interacting with the SAR signal (Dobson, Pierce, and Ulaby, 1996). The greater the degree of difference between backscatter intensities in the reference and those in the posthurricane SAR scenes, the more likely the change detection would forecast a change in site inundation.

As flood depth decreased with time following the surge peak, differences between backscatter intensities decreased, causing damping of the SAR intensity contrast in the reference and posthurricane imagery and, consequently, degrading the performance of inundation mapping. This degradation was most apparent in inundation extents based on ASAR data. As flood depths decreased, there was a general decrease in correspondence between ground-based and ASAR-based measurements of inundation, dropping to 50% or lower at flood depths less than 30 cm. In contrast, at even shallower flood depths, inundations based on PALSAR corresponded 91% of the time with inland hydrographic recordings. The enhanced performance in detecting subcanopy flooding with L-band SAR sensors was most likely due to the higher potential of L-band sensors to penetrate the canopy, particularly in denser canopies (Hong, Wdowinski, and Kim, 2010; Kasischke *et al.,* 2003; Ramsey, 1998; Töyra and Pietroniro, 2005).

Although higher flood levels increased performance of ASAR inundation mapping based in the western and eastern regions, performance in the central region seemed to show a contrary tendency. Using the 17 September 2008 ASAR scene, occurrences of flooding associated with ground-based water-level measurements averaging 13 cm in the central region were correctly mapped 88% of the time. In contrast, using the 14 September ASAR scene to map inundation at the same ground-monitoring sites, there was a correspondence rate of only 50%, which was associated with higher flood depths averaging 59 cm.

One important distinction of the central region (compared to the eastern and western regions) is that palustrine instead of estuarine marshes dominate along shore. In addition, the reference ASAR scenes visually exhibited relatively low SAR

Table 5. *Marsh dieback severity in the intermediate–brackish and saline marsh zones within estuarine wetlands in the eastern region of Louisiana.*

Dieback Severity	Saline Marsh		Intermediate–Brackish Marsh		Total Area (km²)
	%	*km²*	*%*	*km²*	
Low impact	72	1256	47	1014	2270
Moderate impact	27	479	47	1001	1480
High impact	1	10	5	118	128
Severe impact	0	2	1	19	21

backscatter in the central region, even though all but one recorded water level was below the marsh surface at the time of ASAR reference scene collection. In the central region, the contrast between satellite-based mapping performance on 14 September and that on 17 September is not explainable by prehurricane inundation problems with inland hydrologic locations.

Barring disproportionate problems in obtaining valid correspondence estimates, only differences related to changes in marsh type and storm-surge history remain. A possible connection that could be linked to marsh type would be severity of storm-surge impact. Even though a storm surge from Hurricane Gustav was not recorded at the NOAA hydrographic station in the central region, the Amerada Pass coastal station 75 km to the east recorded a 1.15-m storm-surge peak associated with landfall (Figure 1 and 3c). Surge waters with elevated salinity could quickly devastate a palustrine marsh while leaving saline marshes largely intact, except for direct physical impacts (*e.g.,* see Barras, 2003). The palustrine marshes of the central region, having already been impacted by the elevated salinity water of Hurricane Gustav, could have rapidly degraded following the storm surge of Hurricane Ike, thus leaving collapsed or highly altered canopies. The surge from Hurricane Ike, or the subsequently delayed inland runoff noted at hydrologic sites in palustrine wetlands farther to the west, could have removed much of the dead and damaged plant material, thus reducing canopy density. Collapse of the marsh canopy and its subsequent removal would change the performance value of satellite-based inundation mapping because of the association between canopy structure (density, orientation, and stalk thickness) and SAR responses from flooded and nonflooded marshes (*e.g.,* see Grings *et al.,* 2005; Kasischke *et al.,* 2003; Pope *et al.,* 1997; Ramsey *et al.,* 1999). In order to answer whether or not changes in the canopy structure caused by storm-surge impacts resulted in the noted differences in the performance value of satellite-based inundation mapping, continuing research is focused on how the structural aspects of marsh canopies influence SAR data and how these aspects vary when using L-band SAR versus C-band SAR data.

Some limitations of satellite-based inundation mapping that we have discussed could have resulted from prehurricane flooding. This type of limitation could have been aggravated by point assessments of areal features or by changes in marsh structure, independently or in combination. However, low performance of ASAR-based mapping in the central region using a scene from 14 September and in the eastern region using a scene from 17 September were ultimately related to the extended delay in posthurricane scene collection. As delay time lengthened, flood occurrences, as detected in the satellite data, became more scattered, isolated, and shallower. Furthermore, in the case of palustrine marshes, while canopy degradation progressed, the performance value of satellite-based inundation mapping decreased.

Complications of Inundation Detection

While some causes for low inundation mapping performance should be alleviated by more frequent SAR scene collection (Ramsey, 1998, 2005), in addition to the marsh collapse previously discussed, we found three cases where the deviation between ASAR-based estimates of inundation extents and ground-based records of water levels may represent more intractable limitations of the inundation mapping based on change detection. These cases occurred in the eastern region where persistent flood maps based on ASAR collections from 14 and 17 September spatially overlapped.

The first case of deviation between ASAR-based flood maps and ground-based water-level records involved an inland estuarine marsh (CRMS0146) at the eastern edge or near range of the 14 September scene and the midrange of the 17 September scene (Figures 2, 4, and 6). Although site-specific water-level records indicated the presence of fairly deep surface flooding (55 cm) in the region on 14 September and shallow flooding (<17 cm) on 17 September, spatially contiguous flooding was only observed on the ASAR imagery acquired on the latter date (Figure 10). In addition, there was conformity between ASAR-based estimates of flooding and site-specific water-level recordings based on the 14 September scene in coastal marshes (CRMS0261 and CRMS4218) approximately 39 km west of CRMS0146 (Figure 4). A quantitative assessment linking the performance of ASAR-based mapping to SAR incident angle was not performed; however, the degradation of mapping performance in the near range of the SAR scene is a possible limitation of the mapping method.

A second case of deviation between SAR-based flood mapping and ground-based water-level records involved backbarrier estuarine marshes surrounding the eastern embayments (*e.g.,* CRMS0311). Excluding marsh situated along the shoreline (*e.g.,* CRMS0374), these backbarrier marshes are often occupied by short (<1 m) stands of *S. alterniflora* (Ramsey and Rangoonwala, 2006). The water level at CRMS0311 at the time of the 14 September ASAR collection was 0.66 m, which could have nearly reached or overtopped the surface of the marsh. When water levels are near or over the top of the marsh surface, the marsh can approach an open-water surface susceptible to wind roughening. As shown in Ramsey *et al.* (1994), SAR backscatter from roughened inland water surfaces can closely resemble the intensity distribution from nonflooded marshes. In addition to CRMS0311, similar features indicating overtopped canopies were exhibited at other sites that were excluded from the validation-of-inundation analysis. Complexities of this type, particularly in storm-surge situations, lower the performance of inundation mapping based on SAR data.

A pertinent example of such complexities includes the passage of a storm front at the time the 14 September ASAR scene was collected (Ramsey *et al.,* 2009b). The roughened water surface resulting from the storm front was captured on the ASAR scene as high backscatter. At CRMS0680, located within this zone, ground-based water-level records indicate a 1.68-m storm surge at the time of the ASAR collection; however, the high backscatter from the abnormally roughened surface did not indicate the occurrence of marsh flooding. In the same way, roughened water surfaces at more exposed coastal marshes (*e.g.,* CRMS0311) can produce incorrect interpretations.

A third case of deviation between ASAR-based flood mapping using the 17 September scene and ground-based water-level records involves a discrepancy between a shoreline site

(CRMS0147) and a marsh site farther inland (CRMS0146) that may be related to differences in marsh type and structure (Figure 4). The estuarine marshes farther inland in the eastern region were dominated by a marsh species type other than *S. alterniflora,* which is dominant in more nearshore marshes. Even though it is labeled as estuarine marsh in the 2007 Louisiana Coastal Marsh–Vegetative Type Map (Sasser *et al.,* 2008), the inland marsh at CRMS0146 is classified as intermediate–brackish in the regional classification protocol (Chabreck, 1970; Sasser *et al.,* 2008). In contrast to the more vertical and sometimes taller *S. alterniflora* canopies occupying the shoreline interface, intermediate–brackish species, such as *Spartina patens* (marshhay cordgrass) and *Schoenoplectus americanus* (American bulrush), can be highly logged to fairly vertical (McKee and Cherry, 2009; Ramsey *et al.,* 2004). As noted at other coastal sites dominated by *S. alterniflora* (*e.g.,* CRMS0147, CRMS0374, CRMS4529), the shallow flooding recorded in ground-based measurements on the 17 September was below the detection limit we estimated for ASAR-based flood mapping. Conversely, shallow flooding in the marshhay cordgrass– or American bulrush–type marshes (*e.g.,* CRMS0146. CRMS0136, CRMS4218, CRMS0261) was detectable with ASAR. Differences in marsh structures (intermediate–brackish vs. saline estuarine marshes) could have caused differences in the performance of ASAR-based inundation mapping. Results implied a shallower inundation detection limit when mapping intermediate–brackish marsh most often typified by marshhay cordgrass or American bulrush than when mapping marshes of the taller *S. alterniflora.*

Marsh Dieback Extent and Severity

Transformation of multispectral VI values of prehurricane and posthurricane data to a single biomass indicator provided a first-order indication of the presence or absence of dieback and allowed us to quantify its spatial extent. By combining the VI change values with prehurricane values into a common classification scheme, we were able to produce a map depicting dieback extents and magnitudes within marshes naturally exhibiting spatial variability in green-biomass percentages of canopy.

When severity classes were cross-tabulated with the two major coastal wetland types—palustrine and estuarine—a close association between dieback and specific wetland types was revealed. For the most part, palustrine and estuarine wetlands were dominantly associated with areas characterized by the low and moderate impact dieback classes; however, compared with estuarine marsh, palustrine marsh included a higher portion of areas characterized by the severest dieback class. In the central region, areas in palustrine marsh that were characterized by the severest dieback class were found at the ocean and wetland interface. Furthermore, the severest dieback class was associated with palustrine marsh exposed to the brunt of two coastal storm surges, in contrast to palustrine marsh located farther to the west or farther inland of hurricane impacts.

The direct exposure of palustrine marshes in the central region to inundation from storm surge did not suggest that

these marshes experienced longer inundation durations associated with Hurricane Ike than the more moderately impacted and more inland palustrine marshes farther west. In fact, inland water-level recordings suggest the opposite (*e.g.,* see data for CRMS1277, Figure 6). The time delay between the storm-surge event and the inland flood occurrence, coupled with the observation (Wayne Sweeny, Louisiana Department of Wildlife and Fisheries, personal communication) that floodwaters were moving seaward, implies that inland palustrine marshes in the western inland region were impacted by lower salinity waters more than by the higher salinity waters that impacted the shorefront marshes in the central region. In addition, as illustrated by hydrographs provided by NOAA CO-OPS (2009), coastal palustrine marshes in the central region were flooded by elevated salinity waters as a result of Hurricanes Gustav and Ike, with the double "hit" compounding the impact severity. Exposure of the nearshore palustrine marshes to elevated salinities resulted in the most dramatic changes in the greenness of palustrine marsh canopy and (most likely) in the canopy structure. Because severely impacted palustrine marshes were not widely located, there is insufficient evidence for further speculation.

Dieback severity in estuarine wetlands showed a distribution different from that in palustrine types. Estuarine wetlands located in the eastern region were associated more with the low impact class than were those wetlands situated farther inland in the eastern region and occurring dominantly in the western region. The former estuarine marshes were dominantly *S. alterniflora,* and the latter were primarily associated with intermediate–brackish marshes. As did the fresh marshes in the central region, the intermediate–brackish marshes of the (inland) eastern and western regions seemed more sensitive to elevated salinities than to inundation duration.

CONCLUSIONS

Persistent flooding related to storm surge throughout the coastal wetlands of Louisiana was mapped with Envisat ASAR and ALOS PALSAR scenes collected before and after Hurricanes Gustav and Ike in 2008. In the western region of coastal Louisiana, collection of ASAR data near the time of peak flooding captured subcanopy flooding in excess of 1 m. The situation was different during subsequent collection dates that depicted the eastern portion of the study area, where receding flood depths of less than 5 cm were encountered. As elapsed time between peak flooding and satellite data collection increased, the detected subcanopy flood depth decreased and the flooding distribution became more scattered.

In estuarine marshes, correspondences between ASAR-based flood mapping and ground-based water-level records ranged from 86 to 92% when flood depths averaged 79 cm and higher and dropped to 50% when flood depths averaged 27 cm. When water levels averaged 22 cm in the same marshes, the performance of PALSAR-based mapping remained high, with a 91% correspondence rate. Differences in inundation mapping performances were likely related to the potential of deeper canopy penetration of PALSAR relative to C-band ASAR. The low performance of ASAR-based inundation mapping when flooding was shallow was further traced to possible differences

in estuarine marsh type and structure. Using ASAR, minimum flood depths detectable in *S. alterniflora* marshes in shoreward locations were estimated to be 20 to 30 cm, whereas in the more inland intermediate–brackish marshes (most likely consisting of marshhay cordgrass or American bulrush), the detectable flood depth decreased to less than 20 cm. Overall, based on the limited comparison and the techniques used, coastal marsh inundation mapping performance was higher with PALSAR than with C-band ASAR data.

In addition to the common problems of assessing the accuracy of aerial mapping performance from point locations, particularly when flooding is shallow and spotted, a number of factors seemed to have complicated the inundation mapping performance. First, storm damage of coastal marsh canopies would change the SAR backscatter, confusing the interpretability of the prestorm and poststorm comparison. This appeared particularly relevant to nearshore palustrine marshes impacted by elevated salinity surge waters. Second, SAR backscatter from wind-roughened water in overtopped marshes can approach backscatter intensities indicative of nonflooded marsh. Third, mapping performance was lowered in the scene near range, where backscatter intensities are at a maximum. Different SAR system configurations (*e.g.,* wavelength, polarization, and incidence angle range) alter SAR backscatter relationships. Making more frequent collections should alleviate inconsistencies related to wind roughening, and the SAR look angle needs to be taken into account when comparing two scene regions located in very different range positions. ASAR-based mapping exhibited more susceptibility to these two latter complications than did PALSAR-based inundation mapping.

Marsh dieback severity resulting from storm-surge–induced flooding was mapped using a VI developed from Landsat TM images collected before and after Hurricanes Gustav and Ike. Within the estuarine zone intermediate–brackish marshes were most often the most severely impacted, while more shoreward estuarine marshes dominated by *S. alterniflora,* which had experienced a similar inundation history, exhibited less severe impact. This may indicate that under similar inundation scenarios, *S. alterniflora* marshes are more tolerant to surge inundation than are intermediate–brackish marshes. In contrast, palustrine marshes close to the ocean suffered the severest impacts. Evidence suggests that severe impact on these nearshore palustrine marshes may have been more a consequence of direct exposure to elevated salinity than a consequence of surge-related flood duration.

The results of our study emphasize the need for a more consistent monitoring strategy in terms of frequency and timeliness of remote sensing data collection. The main limitation of our approach to inundation mapping using satellite-based SAR data was related to inadequate frequency of image collection. We found that the closer the time between when the SAR data were collected and when the storm-surge peak occurred, the more reliable the detection of maximum flood extents and depths, whereas increased lag time between storm-surge peak and SAR collection led not only to a decrease in the spatial uniformity of flooding but also to a weakening of the link between marsh dieback and casual agent—surge-related water logging and elevated salinities. A secondary

limitation of our approach was a lack of specific information concerning marsh canopy structure and the dynamics that affect it over time and space. As these variables are better understood and their influences on the determination of subcanopy flooding and marsh condition are better determined, the performance of satellite-based mapping of inundation will improve.

ACKNOWLEDGMENTS

LITERATURE CITED

Alaska Satellite Facility. MapReady Remote Sensing Software. 2011. http://www.asf.alaska.edu/sardatacenter/softwaretools (accessed September 8, 2011).

Barras, J., 2003. Change to Cote Blanche Hydrologic Restoration Area (TV-04) after Hurricane Lili. Lafayette, Louisiana: U.S. Geological Survey National Wetlands Research Center, USGS-NWRC 2003-11-112, scale 1: 1,900,000, 1 sheet.

Berg, R., 2009. Tropical Cyclone report Hurricane Ike (AL092008) 1 to 14 September 2008. Miami, Florida: National Oceanic and Atmospheric Association National Hurricane Center. http://www.nhc.noaa.gov/pdf/TCR-AL092008_Ike_3May10.pdf (accessed September 1, 2010).

Beven, J. and Kimberlain, T., 2009. Tropical Cyclone report Hurricane Gustav (AL072008) 25 August to 4 September 2008. Miami, Florida: National Oceanic and Atmospheric Association National Hurricane Center. http://www.nhc.noaa.gov/pdf/TCR-AL072008_Gustav.pdf (accessed September 1, 2010).

Bevington, P., 1969. *Data Reduction and Error Analysis for the Physical Sciences*. New York: McGraw-Hill, 336p.

Chabreck, R., 1970. Marsh Zones and Vegetative Types in the Louisiana Coastal Marshes. Baton Rouge, Louisiana: Louisiana State University, Ph.D. thesis, 112p.

Dobson, C.; Pierce, L., and Ulaby, F., 1996. Knowledge-based land-cover classification using ERS-11JERS-1 SAR composites. *IEEE Transactions on Geoscience and Remote Sensing,* 34(1), 83–99.

Fisher, J. and Mustard, J., 2007. Cross-scalar satellite phenology from ground, Landsat, and MODIS data. *Remote Sensing of Environment,* 109, 261–273.

Grings, F.; Ferrazzoli, P.; Karszenbaum, H.; Tiffenberg, J.; Kandus, P.; Guerriero, L., and Jacobo-Berrles, J., 2005. Modeling temporal evolution of Junco marshes radar signatures. *IEEE Transactions on Geoscience and Remote Sensing,* 43(10), 2238–2245.

Hong, S.; Wdowinski, S., and Kim, S., 2010. Evaluation of TerraSAR-X observations for wetland InSAR application. *IEEE Transactions on Geoscience and Remote Sensing,* 48(2), 864–873.

Kasischke, E.; Smith, K.; Bourgeau-Chavez, L.; Romanowicz, E.; Brunzell, S., and Richardon, C., 2003. Effects of seasonal hydrologic patterns in south Florida wetlands on radar backscatter measured from ERS-2 SAR imagery. *Remote Sensing of Environment,* 88, 423–441.

Kiage, L.; Walker, N.; Balasubramanian, S.; Babin, A., and Barras, J., 2005. Applications of Radarsat-1 synthetic aperture radar imagery to assess hurricane-related flooding of coastal Louisiana. *International Journal of Remote Sensing,* 26(24), 5359–5380.

Klemas, V., 2005. Resolution requirements for coastal applications of new geostationary satellites. *In: Balancing on the Edge—Coastal*

Zone '05. Proceedings of the 14th Biennial Coastal Zone Conference (U.S. National Oceanic and Atmospheric Administration, Coastal Services Center, New Orleans, Louisiana), 5p. https://www.csc. noaa.gov/cz/CZ05_Proceedings/pdf%20files/Klemas.pdf (accessed September 8, 2011).

Klemas, V.; Dobson, J.; Ferguson, R., and Haddad, K., 1993. A coastal land cover classification system for the NOAA Coastwatch Change analysis project. *Journal of Coastal Research,* 9(3), 862–872.

LOSCO (Louisiana Oil Spill Coordinator's Office), 2007. *Louisiana GIS Digital Map of May 2007*. Baton Rouge, Louisiana: LOSCO, digital versatile disc.

Lu, Z. and Kwoun, O., 2008. Radarsat-1 and ERS interferometric analysis over southeastern coastal Louisiana: implication for mapping water-level changes beneath swamp forests. *IEEE Transactions on Geoscience and Remote Sensing,* 46(4), 2167–2184.

McKee, K. and Cherry, J., 2009. Hurricane Katrina sediment slowed elevation loss in subsiding brackish marshes of the Mississippi river delta. *Wetlands,* 29(1), 2–15.

Morton, R.; Bernier, J.; Barras, J.; and Ferina, N.; 2005. Rapid Subsidence and Historical Wetland Loss in the Mississippi Delta Plain: Likely Causes and Future Implications. U.S. Geological Survey, Open-File Report 2005-1216, 124p.

Neyland, R., 2007. The effects of Hurricane Rita on the aquatic vascular flora in a large fresh-water marsh in Cameron Parish, Louisiana. *CASTANEA,* 72(1), 1–7.

NOAA CO-OPS (National Oceanic and Atmospheric Administration Center for Operational Oceanographic Products & Services). Tides & Currents. http://tidesandcurrents.noaa.gov/gmap3/ (accessed September 13, 2009).

PCI Geomatics, 1998. *Using PCI Software, Version 6.3 EASZIPACE (software documentation)*. Richmond Hill, Ontario, Canada: PCI Geomatics.

Pope, K.; Rejmankova, E.; Paris, J., and Woodruff, R., 1997. Detecting seasonal flooding cycles in marshes of the Yucatan Peninsula with SIR-C polarimetric radar imagery. *Remote Sensing Environment,* 59, 157–166.

Ramsey III, E., 1998. Radar remote sensing of wetlands. *In:* Lunetta, R. and Elvidge, C. (eds.), *Remote Sensing Change Detection: Environmental Monitoring Methods and Applications*. Ann Arbor, Michigan: Ann Arbor Press, pp. 211–243.

Ramsey III, E., 2005. Remote sensing of coastal environments. *In:* Schwartz, M. (ed.), *Encyclopedia of Earth Sciences Series*. Dordrecht, the Netherlands: Kluwer Academic, pp. 797–803.

Ramsey III, E. and Rangoonwala, A., 2006, Site-specific canopy reflectance related to marsh dieback onset and progression in coastal Louisiana. *Photogrammetric Engineering and Remote Sensing,* 72(6), 641–652.

Ramsey III, E.; Laine, S.; Werle, D.; Tittley, B., and Lapp, D., 1994. Monitoring Hurricane Andrew damage and recovery of the coastal Louisiana marsh using satellite remote sensing data. *In:* Wells, P. and Ricketts, P. (eds.), *Proceedings of the Coastal Zone, Canada '94* (Hallifax, Canada), pp. 1841–1852.

Ramsey III, E.; Lu, Z.; Suzuoki, Y.; Rangoonwala, A., and Werle, D., 2011. Monitoring duration and extent of storm surge flooding along the Louisiana coast with Envisat ASAR data. *IEEE Geoscience and Remote Sensing,* 4(2), 387–399.

Ramsey III, E.; Nelson, G.; Baarnes, F., and Spell, R., 2004. Light attenuation profiling as an indicator of structural changes in coastal marshes. *In:* Lunetta, R. and Lyon, J. (eds.), *Remote Sensing and GIS Accuracy Assessment*. New York: CRC Press, pp. 59–73.

Ramsey III, E.; Nelson, G.; Sapkota, S.; Laine, S.; Verdi, J., and Krasznay, S., 1999. Using multiple polarization L band radar to monitor marsh burn recovery. *IEEE Transactions on Geoscience and Remote Sensing,* 37(1), 635–639.

Ramsey III, E.; Rangoonwala, A.; Middleton, B., and Lu, Z., 2009a. Satellite optical and radar image data of forested wetland impact on and short-term recovery from Hurricane Katrina in the lower Pearl River flood plain of Louisiana, USA. *Wetlands,* 29(1), 66–79.

Ramsey III, E.; Werle, D.; Lu, Z.; Rangoonwala, A., and Suzuoki, Y., 2009b. A case of timely satellite image acquisitions in support of coastal emergency environmental response management. *Journal of Coastal Research,* 25(5), 1168–1172.

Sasser, C.; Visser, J.; Mouton, E.; Linscombe, J., and Hartley, S., 2008. Vegetation types in coastal Louisiana in 2007. U.S. Geological Survey Open-File Report 2008-1224, 1:550,000 scale, 1 map sheet.

SONRIS (Strategic Online Natural Resources Information System). Welcome to SONRIS. http://sonris-www.dnr.state.la.us/www_root/ sonris_portal_1.htm (accessed September 2, 2010).

Tou, J. and Gonzalez, R., 1974. *Pattern Recognition Principles*. Reading, Massachusetts: Addison-Wesley.

Töyra, J. and Pietroniro, A., 2005. Towards operational monitoring of a northern wetland using geomatics-based techniques. *Remote Sensing of Environment,* 97, 74–191.

USACE (U.S. Army Corps of Engineers) Mississippi Valley Division, 2006. Enhancing landscape integrity in coastal Louisiana: water, sediment & ecosystems. http://www.mvd.usace.army.mil/lcast/pdfs/ CEM2.pdf (accessed August 31, 2010).